

6-1-2002

Dynamic Multiphysics Model for Solar Array

Shengyi Liu
Boeing, shengyi.liu@boeing.com

Roger A. Dougal
University of South Carolina - Columbia, dougal@enr.sc.edu

Follow this and additional works at: https://scholarcommons.sc.edu/elct_facpub



Part of the [Electrical and Computer Engineering Commons](#)

Publication Info

Published in *IEEE Transactions on Energy Conversion*, Volume 17, 2002, pages 285-294.

This Article is brought to you by the Electrical Engineering, Department of at Scholar Commons. It has been accepted for inclusion in Faculty Publications by an authorized administrator of Scholar Commons. For more information, please contact digres@mailbox.sc.edu.

Dynamic Multiphysics Model for Solar Array

Shengyi Liu, *Member, IEEE* and Roger A. Dougal, *Senior Member, IEEE*

Abstract—An approach to model the solar cell system with coupled multiphysics equations (photovoltaic, electro-thermal, direct heating and cooling processes) within the context of the resistive-companion method in the Virtual Test Bed computational environment is presented. Appropriate across and through variables are defined for the thermal terminal of the system so that temperature is properly represented as a state variable, rather than as a parameter of the system. This allows enforcement of the system power conservation through all terminals, and allows simultaneous solutions for both the electrical potentials and the system temperature. The thermal port built accordingly can be used for natural thermal coupling.

The static and dynamic behaviors of the solar array model based on the approach are obtained and validated through comparison of simulation results to theoretical predictions and other reported data. The electro-thermal modeling method developed here can be generally used in the modeling of other devices, and the method to define the across and through variables can also be generalized to any other interdisciplinary processes where natural coupling is required.

Index Terms—Electro-thermal modeling, resistive companion method, solar energy conversion, Virtual Test Bed simulation.

NOMENCLATURE

A	Area (in square meters).	I_{sat}	Junction saturation current (in amperes).
$B(t-h)$	History vector.	I_{sat0}	Junction saturation current at temperature T_0 (in amperes).
$b_n(t-h)$	History for node n .	I_{sc}	Short-circuit current (in amperes).
C	Temperature coefficient of light-induced current (in amperes per degrees Kelvin).	i	Solar cell current (in amperes).
c_p	Specific heat (in joules per kilogram per degrees Kelvin).	i_d	Junction current (in amperes).
D	Pulsed power load duty ratio.	i_n	Terminal through variable at node n .
d	Cell thickness (in meters).	i_P	Light terminal through variable.
$E(\lambda)$	Solar spectral irradiance (in watts per square meter per micrometer).	i_T	Thermal terminal through variable (in watts per degrees Kelvin).
E_g	Band gap (in electrovolts).	J_{sat0}	Junction saturation current density at T_0 (in amperes per square meter).
E_{g0}	Band gap at a reference temperature T_0 (in electrovolts).	k	Boltzmann constant.
e	Electronic charge.	m	Mass (in kilograms), also for node numbers.
f	Pulsed power load frequency (in Hertz).	n	Node numbers.
G	Conductance matrix.	P	Solar irradiance (in watts per square meter).
g_{mn}	Conductance of node m with respect to node n .	P_0	Solar irradiance at reference temperature T_0 (in watts per square meter).
h	Time step (in seconds).	Q	Power (in watts).
h_c	Cooling coefficient (in watts per square meter per degrees Kelvin).	Q_e	Electrical power (in watts).
$I(t)$	Terminal through variable vector.	Q_T	Thermal power (in watts).
I_P	Light-induced current (in amperes).	R_s	Intrinsic series resistance of the solar cell (in ohms).
		R_{sh}	Intrinsic shunt resistance of the solar cell (in ohms).
		T	Temperature (in degrees Kelvin).
		T_a	Ambient temperature (in degrees Kelvin).
		T_0	Reference temperature (in degrees Kelvin).
		t	Independent time variable (in seconds).
		$V(t)$	Terminal across variable vector.
		v	Cell voltage (in volts).
		v_d	Junction voltage (in volts).
		v_n	Terminal across variable at node n .
		v_{th}	Junction thermal potential (in volts).
		$\delta I_{P,T}$	The light-induced current due to temperature variation (in amperes).
		ε	Emissivity.
		γ	Junction ideality factor.
		η	Quantum efficiency.
		η_e	Energy conversion efficiency.
		λ	Photon wavelength (in micrometers).
		τ	Light transmission coefficient.
		ρ	Reflection coefficient.
		\mathfrak{R}	Spectral dependent responsivity (in amperes per watt).
		$\bar{\mathfrak{R}}$	Spectral averaged responsivity (in amperes per watt).

Manuscript received October 1, 2001; revised February 25, 2002. This work was supported by Veridian MRJ under Contract 00-MRJ-1085-100.

The authors are with the Electrical Engineering Department, University of South Carolina, Columbia, SC 29208 USA (e-mail: lius@enr.sc.edu; Dougal@enr.sc.edu).

Publisher Item Identifier S 0885-8969(02)05416-5.

I. INTRODUCTION

ENERGY conversion in a solar cell includes two fundamental processes:

- 1) a photovoltaic process that converts the light into electricity;

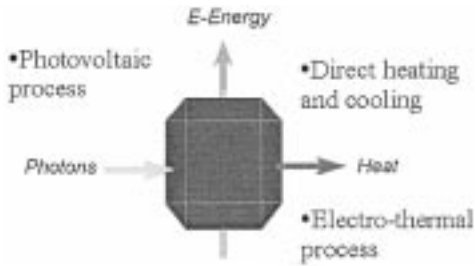


Fig. 1. Energy conversion processes, direct heating, and cooling processes in a solar cell.

- 2) an electrothermal process that turns some of the electric energy into heat.

In addition, there are direct heating processes due to absorption of the solar spectral irradiance outside the region of photovoltaic effect, heating due to recombination losses, and cooling processes due to conduction, radiation and convection, as illustrated in Fig. 1. The properties of the junction of a solar cell through which the photovoltaic process takes place are strongly temperature-dependent. Therefore, it is important to model the many physical processes as a whole in order to precisely predict the dynamic response of the solar cell.

Traditionally, the thermal process of an electric device is modeled by a separate thermal network, employing the concepts of thermal resistance (due to a finite thermal conductivity) and thermal capacitance (due to heat capacity of the device mass) [1]–[6]. The analogous relationships between electrical and thermal circuits make this easy to do in a standard circuit simulator. Here, temperature corresponds to voltage, and heat power to current. However, because heat power is used as the through variable in the conventional thermal network, the thermal terminal cannot be used for natural thermal coupling (the product of the across variable—temperature, and the through variable—heat power, does not equal to power). In the present work, we are seeking a thermal terminal that can be used for natural heat power transport, so that the system power conservation can be observed, and the inter-disciplinary processes in the system can be modeled uniformly based on the fully coupled multiphysics equations. To accomplish that, appropriate across and through variables are defined first for each individual terminal based on the natural conservation laws for the pertinent physical processes. Secondly, the device equations are formulated in a way that allows simultaneous solution for all across variables of the system, including the electric potentials and the temperatures. Here, we formulate those equations in resistive-companion form (RC) [7], and then demonstrate the implementation and results in the virtual test bed (VTB) [8] environment.

The rest of this paper is organized as follows. The mathematical descriptions of the physical processes in a solar cell are given in Section II. The RC model formulation for those processes is derived in Section III, with particular attention to the details of the thermal terminal. Section IV illustrates the results obtained by applying the simulation model in a particular system and provides validation of the model. The conclusions are made in Section V.

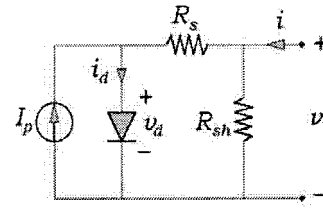


Fig. 2. Equivalent circuit for the electrical characteristics of a solar cell.

II. SYSTEM DESCRIPTIONS OF SOLAR CELL

Three distinct energy forms are involved in photovoltaic solar energy conversion: light, electricity and heat, as was shown in Fig. 1. The mathematical descriptions for the conversion processes and the inter-relationships between the different energy forms will be discussed in detail.

A. Photovoltaic Process

The processes involved in conversion of light into electric energy in a semiconductor photovoltaic cell (or a solar cell) are well known and documented [9]–[15], so we will only briefly summarize them here. In describing the electrical characteristics of a solar array, a physics-circuit oriented approach [10], [12], [14], [15] is prevalent in the literature and proved to be effective, so it will be used here. The equivalent circuit of a solar array, shown in Fig. 2, has four components: a light-induced current source I_P , a diode parallel to the source, a series resistor R_s and a shunt resistor R_{sh} . The light-induced current is due to the separation and drift of the photon-generated electron-hole pairs under the influence of the built-in field. This current is directly proportional to the irradiance. For a given cell material, it is expressed as

$$I_P(t) = \overline{\mathfrak{R}}AP(t) + \delta I_{P,T}(t) \quad (1)$$

where $P(t)$ is the solar irradiance in W/m^2 , A is the active area in m^2 , and $\overline{\mathfrak{R}}$ is the spectral-averaged responsivity [16] in A/W , which is given as

$$\overline{\mathfrak{R}} = \frac{\int_0^{\lambda(E_g)} \mathfrak{R}(\lambda) E(\lambda) d\lambda}{\int_0^{\infty} E(\lambda) d\lambda} \quad (2)$$

where $E(\lambda)$ is the solar irradiance spectral distribution function, and $\lambda(E_g)$ is the wavelength corresponding to the band gap. The responsivity depends not only on the cell material, but also on the weather conditions since the wavelength distribution of the irradiance varies as sunlight passes through the atmosphere. The standard spectral irradiance functions for different air masses [17] can be used to evaluate the averaged responsivity for given cell materials. For solar cells in space applications, the spectral irradiance corresponds to air mass 0 conditions.

In equation (1), $\delta I_{P,T}(t)$ is the light-induced current change due to temperature variation. The band gap decreases at higher temperatures, which effectively increases the number of photons that can create electron-hole pairs. In the meantime, higher temperatures reduce the diffusion length and lifetime of carriers, therefore they increase recombination loss [18]–[20]. The net effect is that the light-induced current slightly increases

at higher temperatures. The temperature correction term to the light-induced current can be approximated as [21]

$$\delta I_{P,T}(t) = C[T(t) - T_0] \frac{P(t)}{P_0} \quad (3)$$

where P_0 is the irradiance at an arbitrary reference temperature T_0 , and C is the temperature coefficient having a value of 0.0017 A/K for a silicon solar cell.

The diode in Fig. 2 represents the p–n junction of the solar cell. Under normal operating conditions, the potential v_d is positive so that the photocurrent I_p produces a net positive power. The diode is forward biased, but conducts only weakly. Physically, the diode current is due to the diffusion of minority carriers in the depletion region, which represents an incomplete collection of electron–hole pairs due to diffusion [13]. The relation of the current to the biasing voltage follows typical ideal diode characteristics [15], as given by

$$i_d(t) = I_{sat}(t) \left(\exp\left(\frac{v_d(t)}{\gamma v_{th}(t)}\right) - 1 \right) \quad (4)$$

where γ is the diode ideality factor, I_{sat} and v_d are the reverse saturation current and the thermal potential, both of which are the function of temperature. The thermal potential is

$$v_{th}(t) = \frac{kT(t)}{e}. \quad (5)$$

The saturation current depends on the type of junction. For a p–n junction, considering that the temperature effect on the saturation current is primarily due to the temperature dependence of intrinsic carrier generation, it can be approximated as [15]

$$I_{sat}(t) = I_{sat0} \left(\frac{T(t)}{T_0} \right)^3 \cdot \exp\left(\frac{e}{\gamma \cdot k} \left(\frac{E_g(T_0)}{T_0} - \frac{E_g[T(t)]}{T(t)} \right)\right). \quad (6)$$

The notations in the last two equations are explained as follows. k is Boltzmann constant, and I_{sat0} is the reverse saturation current at an arbitrary reference temperature T_0 .

The output current from the solar cell is a net result of the drift current of carriers due to the built-in potential, the reverse diffusion current due to the carrier concentration gradient, and the leakage current due to shunt resistance. Considering the equivalent circuit shown in Fig. 2, the relation between the solar cell terminal current and voltage can then be found as

$$i(t) = \frac{1}{R_s} \left(v(t) - \gamma v_{th}(t) \right) \cdot \ln \left(\frac{I_p(t) + i(t) - \frac{v(t)}{R_{sh}}}{I_{sat}(t)} + 1 \right) + \frac{v(t)}{R_{sh}}. \quad (7)$$

Equations (1), (4), and (7) constitute the descriptions of the photovoltaic processes.

B. Electro-Thermal Process

The electro-thermal process and heating/cooling process of a solar cell is governed by its energy balance equation. The rate of

change of the cell internal energy equals to the net heat power absorbed by the cell. This can be expressed as

$$m c_p \frac{dT(t)}{dt} = \frac{[v(t) - v_d(t)]^2}{R_s} + \frac{[v(t)]^2}{R_{sh}} + i_d(t) v_d(t) + (1 - \rho - \tau - \eta) A P(t) - \sum h_c(t) A [T(t) - T_a] \quad (8)$$

where m is the mass in kilograms, c_p is the specific heat of the cell in J/(kgK). ρ is the irradiance reflection coefficient of the cell surface, τ is the irradiance transmission coefficient of the cell, and η is the quantum efficiency [16] of the photovoltaic process. The first three terms on the right-hand side represent internal losses due to ohmic heating in the series and shunt resistances, and due to incomplete carrier collection resulting from diffusion current [13], [15]. Notice that, the specific heat and the electrical conductivity of the cell are in general functions of temperature. However, to a first approximation, we will assume they are constant in the range of our interest. The fourth term is the direct heating from the sun. The direct heating is equal to the total solar power incident on the cell surface $AP(t)$, minus the reflected power $\rho AP(t)$, the power transmitted entirely through the device $\tau AP(t)$, and the optical power $\eta AP(t)$ that contributes to the light-induced current. Notice that ρ , τ and η are all spectrally-averaged values. For the best solar energy conversion performance, the quantum efficiency should be increased; while the reflection and transmission coefficients should be reduced as much as possible for the photons of energies higher than the band gap, and they should be increased as much as possible for the photons having energies lower than the band gap. Depending upon particular designs, advanced technologies (e.g., coating and texturing on the surfaces [22]) can be used to increase the conversion efficiency and to reduce direct heating. The last term is the heat power loss due to cooling mechanisms such as conduction through the heat sink, and radiation and convection from the cell front surface. T_a is the ambient temperature. The effective cooling coefficient h_c is specific to each mechanism, and it is in general a function of temperature.

Equation (8) assumes a lumped thermal model of the solar cell. Heat is mainly generated on the near-surface layer where the events of electron–hole pair generation and recombination, current flow and absorption of direct heating take place. Most of the generated heat is then conducted through the substrate to the heat sink. Convection and radiation carry heat away from the front surface of the solar cell and from the heat sink. Here, the temperature of the solar cell is that of the bulk of the cell active layer and the substrate.

Equations (1)–(8) complete the mathematical descriptions of the interdisciplinary system—the solar cell.

III. RC MODEL FORMULATION

The resistive-companion method provides a way to account for natural conservation laws by defining a pair of across and through variables at each terminal. The device object interacts with the VTB network solver by providing the device conductance matrix and the history vector in each simulation time step, so that the solution to the entire circuit can be sought by the solver based on the mathematical equivalent of a nodal circuit analysis. The solver requires that the relations of the terminal

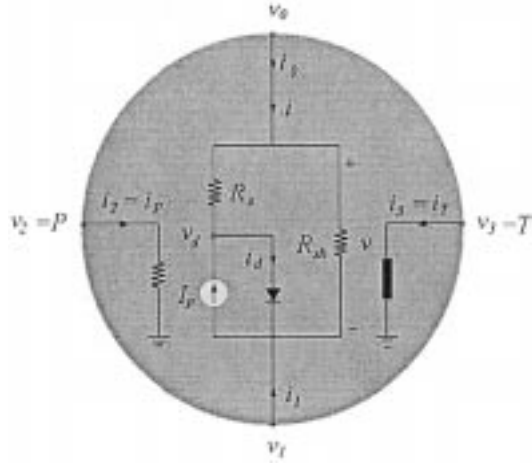


Fig. 3. Circuit representation of the equations that describe the physics of a solar cell.

variables for each device be written in the following standard form:

$$I(t) = G \cdot V(t) - B(t-h) \quad (9)$$

where $I(t)$ is the through variable vector, $V(t)$ is the across variable vector, G is the conductance matrix, $B(t-h)$ is the history vector of the device, and h is the simulation time step. Notice that although the term “conductance matrix,” inherited from electric network analysis, is used, the terminal variables are more generally across and through variables, not necessarily voltage and current. As stated previously, one of goals of this paper is to define appropriate terminal variables so that natural thermal coupling can be achieved.

To build an RC model for a solar cell, it is helpful to use the illustration in Fig. 3. It shows that the solar cell interacts with the external world through its four terminals. Nodes 0 and 1 are electric terminals through which the cell provides electric power to the load. Node 2 is a light terminal that receives irradiance from the sun. Node 3 is a thermal terminal that allows carrying heat energy into or out of the solar cell via conduction, convection and radiation. The circuit network shown in the cell chip—an imagined built-in circuit that is governed by (1)–(8), characterizes the interrelations of the terminals. Note that the circuit drawn on the semiconductor wafer represents the physical processes of the solar cell. It is not an actual physical layout of any circuit of the solar cell. At this point, the conductances for nodes 2 and 3 have not yet been defined. The conductance for each terminal will be found as the RC model equations are derived. In fact, the circuit network itself is the direct result of RC model equations. Although a circuit representation can always be drawn for a nonelectrical system based on the RC equations, it is neither imperative nor necessary to do so if the circuit confuses the nature of that physical system (e.g., a mechanical shaft, a fluid stream or a chemical system). Here we use a circuit to illustrate the modeling procedures because it is simply intuitive and instructive for that purpose, and familiar to this audience.

A. Electrical Terminals

The circuit between nodes 0 and 1 in Fig. 3 is a copy of that in Fig. 2, except that the terminal variables are assigned to each node. Naturally, the terminal variables for these two nodes are the electric potentials and the currents. Notice that the convention for positive current direction is into the node. It can be seen that

$$i(t) = i_0(t) = -i_1(t) \quad (10)$$

$$v(t) = v_0(t) - v_1(t). \quad (11)$$

The terminal currents depend on the node voltages at 0 and 1, and also on the irradiance P and the temperature T (the across variables at nodes 2 and 3; P and T are also used as subscripts to denote the names of the corresponding nodes). The standard RC equations follow that

$$\begin{pmatrix} i_0(t) \\ i_1(t) \end{pmatrix} = \begin{pmatrix} g_{00} & g_{01} & g_{0P} & g_{0T} \\ g_{10} & g_{11} & g_{1P} & g_{1T} \end{pmatrix} \begin{pmatrix} v_0(t) \\ v_1(t) \\ P(t) \\ T(t) \end{pmatrix} - \begin{pmatrix} b_0(t-h) \\ b_1(t-h) \end{pmatrix} \quad (12)$$

where the conductance elements can be found as

$$g_{mn} = \left(\frac{\partial i_m}{\partial v_n} \right)_{t-h}, \quad \text{for } m = 0, 1, \text{ and } n = 0, 1, P, T. \quad (13)$$

To find the history vector, the first order Taylor expansion is applied to approximate equation (7). This yields

$$\begin{aligned} i_0(t) &= i_0(t-h) + g_{00}\Delta v_0(t-h) + g_{01}\Delta v_1(t-h) \\ &\quad + g_{0P}\Delta P(t-h) + g_{0T}\Delta T(t-h) \\ &= g_{00}v_0(t) + g_{01}v_1(t) + g_{0P}P(t) + g_{0T}T(t) \\ &\quad + i_0(t-h) - g_{00}v_0(t-h) - g_{01}v_1(t-h) \\ &\quad - g_{0P}P(t-h) - g_{0T}T(t-h). \end{aligned} \quad (14)$$

Notice that equation (14) is already in the standard form. The history for i_0 is

$$\begin{aligned} b_0(t-h) &= -i_0(t-h) + g_{00}v_0(t-h) + g_{01}v_1(t-h) \\ &\quad + g_{0P}P(t-h) + g_{0T}T(t-h). \end{aligned} \quad (15)$$

Applying equation (10), it can be found that

$$b_1(t-h) = -b_0(t-h). \quad (16)$$

B. Light Terminal

The interaction of the electrical circuit with the light terminal is specified by equation (1)—the light-induced current is linearly proportional to the solar irradiance that is an input quantity for the solar cell system. Since the solar irradiance is not a function of either the cell junction properties or the load conditions it is therefore appropriate to treat the irradiance as a signal input. (While future versions of the VTB computational system will comply with IEEE VHDL-AMS standards [23] with respect to object coupling methods: natural coupling, signal coupling and data coupling, the current release version of VTB treats all ports as natural ports. We therefore implement a signal port for the RC solver by specifying a low but not zero input conductance that negligibly loads the irradiance “source.” This finite input

TABLE I
TERMINAL COMPARISONS

Terminal	Notation	Quantity	Unit
Electric terminal	v	electric potential (across variable)	V
	i	Current (through variable)	A (W/V)
	Q_e	Electric power	W
	T	Temperature (across variable)	K
Thermal terminal	i_T	thermal current (through variable)	W/K
	Q_T	Thermal power	W

conductance is shown at the left of the circuit in Fig. 3.) Since the current into a signal port should ideally be zero, assigning a through variable to this terminal is simply for the convenience of writing the RC equation, which is given as

$$i_P(t) = \begin{pmatrix} 0 & 0 & \frac{1}{R_P} & 0 \end{pmatrix} \begin{pmatrix} v_0(t) \\ v_1(t) \\ P(t) \\ T(t) \end{pmatrix} - (0) \quad (17)$$

where, R_P , is the input resistance of the light terminal, which should be very large so as not to “load” the solar source.

C. Thermal Terminal

We use here temperature as the state variable that defines the internal energy of the solar cell system. This is a reasonable assumption because change of the mass density hence change of the specific volume of the solar cell is minimal during the normal operation range of the temperature from 200 K to 400 K. Like an electric potential difference causing electric power flow, a temperature difference results in thermal power flow, hence it is natural to identify temperature as the across variable. However, unlike an electric terminal that transports power ($Q_e = i \cdot v$), the conventionally defined thermal terminal does not transport power if heat power is used as the through variable because $Q_T \neq Q_T \cdot T$. Thus Q_T is not an appropriate choice of through variable for natural thermal coupling. We overcome the problem by defining the thermal through variable i_T so that the following equation is enforced

$$Q_T = i_T \cdot T. \quad (18)$$

That is to say, a heat power Q_T will be produced if a thermal through variable of a quantity i_T flows into a terminal at a temperature T . The unit of i_T is thus W/K. To further explain equation (18), Table I lists corresponding quantities for electric and thermal terminals.

Now a natural thermal coupling terminal can be established by applying equation (18). The energy balance equation, replacing the heat loss terms in equation (8) by the heat power transferred through the terminal, now is

$$c_p m \frac{dT(t)}{dt} = \frac{[v(t) - v_d(t)]^2}{R_s} + \frac{[v(t)]^2}{R_{sh}} + i_d(t)v_d(t) + (1 - \rho - \tau - \eta)AP(t) + i_T(t)T(t). \quad (19)$$

Again, by convention, a positive value of the through variable represents flow into the node. Note that all heat energy is removed from the solar array through the thermal terminal, regardless of the heat dissipation mechanism. So if radiative cooling is significant, a radiator model can be attached to the thermal port. If convective cooling is important a convective cooling model can be connected, in addition to, or instead of, the radiator model, and so forth for other mechanisms.

To obtain the RC equation for the terminal, equation (19) is discretized within one time step using trapezoidal method. Solving for $i_T(t)$, yields

$$i_T(t) = \frac{hc_p m}{2} - \left(\frac{hc_p m}{2} + i_T(t-h) \right) \frac{T(t-h)}{T(t)} - \frac{[v(t) - v_d(t)]^2 + [v(t-h) - v_d(t-h)]^2}{R_s T(t)} - \frac{[v(t)]^2 + [v(t-h)]^2}{R_{sh} T(t)} - \frac{i_d(t)v_d(t) + i_d(t-h)v_d(t-h)}{T(t)} - \frac{(1 - \rho - \tau - \eta)A[P(t) + P(t-h)]}{T(t)}. \quad (20)$$

The RC equation is found by following the procedures used in part A to get

$$i_T(t) = \begin{pmatrix} g_{T0} & g_{T1} & g_{TP} & g_{TT} \end{pmatrix} \begin{pmatrix} v_0(t) \\ v_1(t) \\ P(t) \\ T(t) \end{pmatrix} - (b_T(t-h)) \quad (21)$$

where

$$g_{Tn} = \left(\frac{\partial i_T}{\partial v_n} \right)_{t-h}, \quad \text{for } n = 0, 1, P, T \quad (22)$$

$$b_T(t-h) = -i_T(t-h) + g_{T0}v_0(t-h) + g_{T1}v_1(t-h) + g_{TP}P(t-h) + g_{TT}T(t-h). \quad (23)$$

The complete RC model equations for the solar cell including natural thermal coupling are then given as

$$\begin{pmatrix} i_0(t) \\ i_1(t) \\ i_P(t) \\ i_T(t) \end{pmatrix} = \begin{pmatrix} g_{00} & g_{01} & g_{0P} & g_{0T} \\ g_{10} & g_{11} & g_{1P} & g_{1T} \\ 0 & 0 & g_{PP} & 0 \\ g_{T0} & g_{T1} & g_{TP} & g_{TT} \end{pmatrix} \begin{pmatrix} v_0(t) \\ v_1(t) \\ P(t) \\ T(t) \end{pmatrix} - \begin{pmatrix} b_0(t-h) \\ b_1(t-h) \\ 0 \\ b_T(t-h) \end{pmatrix}. \quad (24)$$

D. Energy Conservation and Efficiency

With the newly defined thermal through variable, it is now possible to write the energy conservation equation for the system in terms of its terminal variables. This is given as

$$(1 - \rho - \tau)AP + iv + i_T T = c_p m \frac{dT}{dt}. \quad (25)$$

The first term on the left-hand side is the net sun power received at the light terminal, the second is the electric power from its electric terminal, and the third is the heat power from the thermal terminal. The net power absorbed equals the rate of change of internal energy. Using equation (19) in (25), the quantum efficiency can be found as

$$\eta = \frac{\frac{[v-v_d]^2}{R_s} + \frac{v^2}{R_{sh}} + i_d v_d - iv}{AP}. \quad (26)$$

Equation (26) explains that the quantum efficiency is a ratio of the sum of the electric power delivered and the internal losses to the total solar power incident on the cell surface. The energy conversion efficiency, defined as the ratio of electric output power to solar input power [11]–[13] can be found, from equation (26), as

$$\eta_e = \frac{-iv}{AP} = \eta - \frac{\frac{[v-v_d]^2}{R_s} + \frac{v^2}{R_{sh}} + i_d v_d}{AP}. \quad (27)$$

One can infer from equation (27) that, under the condition of no ohmic or diffusion losses, the conversion efficiency equals the quantum efficiency, and we have $i = -I_P$, $v = v_d$. Therefore

$$\eta = \frac{I_P v_d}{AP}. \quad (28)$$

Although equation (28) is derived from a special case, it applies to all conditions of solar cell operation (except the open-circuit case). It simply says that the quantum efficiency is the ratio of the power carried by light-induced current to the total solar power irradiated on the cell surface. Equation (28) will be used in the energy balance equation (19) for the device thermal modeling.

TABLE II
PARAMETERS FOR SILICON SOLAR CELL

Parameter	Unit	Value	
		AM0	AM1
E_{g0}	eV	1.106	
J_{sat0}	A/m ²	1.35×10^{-7}	
γ		1.13	1.0
$\overline{\mathcal{R}}$	A/W	0.379	0.305
A	m ²	0.01	
R_s	Ω	0.0432	0.0113
R_{sh}	Ω	5k	
m	kg	0.117	
c_p	J/kg/ K	712	

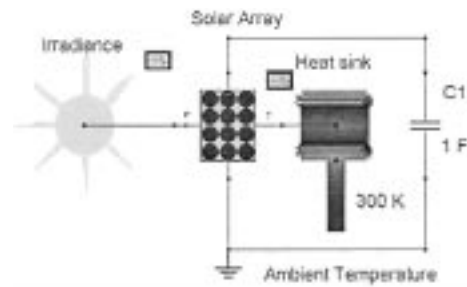


Fig. 4. Circuit to test the operating characteristics of the solar array.

IV. VTB SIMULATION

The example model is for a single-junction silicon cell with a 10 cm × 10 cm light-sensitive area. The array is also assumed to have a light tracking system, and anti-reflection techniques on the front surface and the reflector on the back surface are used in the cell so that the reflection and transmission coefficient are nearly zero. Some typical values [15] of the cell parameters that are used in the model are listed in Table II. Note that the ideality factor γ and the series resistance R_s are used as fitting parameters since the junction properties largely depend on the details of the material microstructures and the manufacturing processes. The energy gap is assumed to have a temperature shift of (-2.3×10^{-4}) eV/K.

A. Solar Array Static Characteristics

Fig. 4 shows a VTB schematic view of the circuit to obtain the static characteristics of the solar array. The array is of 10 × 10 cells, each of which has the parameters listed in Table II. The irradiance model provides to the array input terminal P an insolation level of 1353 W/m² when set to AM0 condition, or 1070 W/m² when set to AM1. The thermal terminal T of the array is connected to a heat sink that carries heat away to the ambient represented by a thermal source. By using a capacitor as the load, the array sweeps through its entire operating range, from short-circuit to open-circuit conditions, so that the operating characteristics ($I \sim V$, $Q \sim V$) are easily obtained in a single simulation. Since the capacitor is charged to an open-circuit voltage in less than 0.3 s (the time constant is about 0.02 s), the operating characteristics so obtained are under the condition

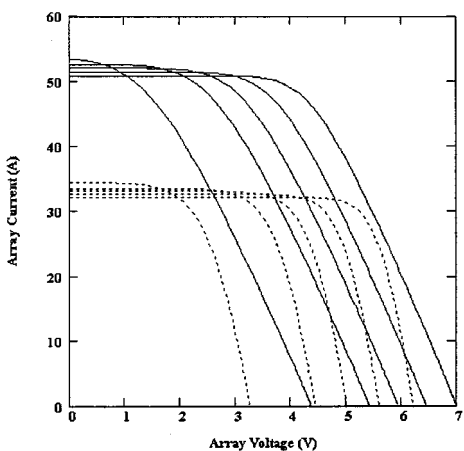


Fig. 5. Array current versus its voltage for the temperatures of (from right to left) 273 K, 300K, 325 K, 350 K, 375 K, and 400 K. Solid lines for AM0 condition, and dotted lines for AM1 condition.

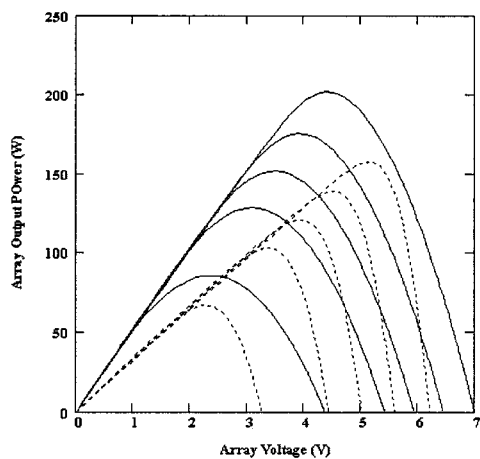


Fig. 6. Array output power versus its voltage for the temperatures of (from right to left) 273 K, 300 K, 325 K, 350 K, 375 K, and 400 K. The solid lines for AM0 condition, the dotted lines for AM1 condition.

of nearly a constant array temperature. Note that the maximum increase of the cell temperature in 0.5 s is 0.08 K for an ambient temperature of 400 K, therefore the effect on the operating characteristics due to temperature variation can be ignored. This insures that the thermal condition is static. The output variables from the array model include the voltage, current, efficiency and temperature that can be used for array performance analysis. The results are explained as follows.

Figs. 5 and 6 shows $I \sim V$ and $Q \sim V$ characteristics obtained from simulation under AM0 insolation level (solid lines) and AM1 insolation level (dotted lines). Notice that although the short-circuit current increases as the temperature increases, the open-circuit voltage decreases at a faster pace, resulting in lower output power. Corresponding to each temperature, there is a maximum power point that can be used as the operating point to extract maximum power from the array. At the maximum power point, the array energy conversion efficiency is at its maximum. The efficiencies predicted by the model are compared to the data from [15] and shown in Fig. 7, where the circles and diamond (overlapped) are data points, and lines are simulation results. As can be seen, the conversion efficiencies are matched very well.

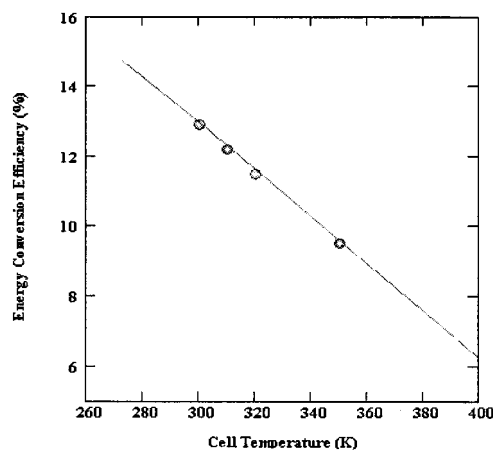


Fig. 7. Comparison of energy conversion efficiency predicted by VTB model (lines for AM0 and AM1 are overlapped) to the data (circles for AM0 and diamonds for AM1 are overlapped) from reference [15].

B. Dynamic Simulation

An integrated photovoltaic power system using a solar array as the main power source was built in the VTB environment, as shown in Fig. 8. Included in the system are a Ni/Cd battery array for energy storage, an ultracapacitor bank for extension of battery discharge life [24], a transmitter as a pulsed power load, a maximum power point tracker (controller, converter and sensor), and a solar irradiance model. Table III lists the setup parameters for all these components.

The power system is assumed located at the latitude $34^{\circ}N$ and longitude $82^{\circ}W$. The sky is assumed clear, and the ambient temperature is 300 K constantly throughout the day. The time of the system operation shown by the simulation results is from 5 AM to 8 PM, June 21, total 15 h. VTB computational environment allows to graphically view the dynamic states of many terminal and internal variables. Here, the results that are most related to the subject of this presentation are summarized in Figs. 9–12, and explained as follows.

Fig. 9 shows the various types of power and relations among them as a function of time. In particular, the graph is used to verify the power conservation on which the solar array model is built. The horizontal scale is expressed as a percentage of total simulated time. 0% is corresponding to 5 AM, while 100% corresponding to 8 PM. From bottom to top, the curves are for the electric output power, the radiated heat power, the convected heat power, the sum of output heat and electric power, and the irradiated solar power. As can be seen, the solar irradiation increases in the morning, and decreases in the afternoon. The array starts to convert the energy when the sun rises at about 5:15 AM, and ceases to make energy when the sun sets at 7:25 PM. During most of the day, about 10.9 to 12.2% of the irradiated solar power is converted to the electric power, while the rest of the solar power is turned to heat and eventually dissipated to the environment through radiation and convection. Notice that in the morning, the sum of the output heat and electric power from the array is less than the irradiated power. The difference results from the absorption of the heat that is stored as internal energy by the array (temperature increase). In the afternoon, the sum of the output heat and electric power from the array is higher than

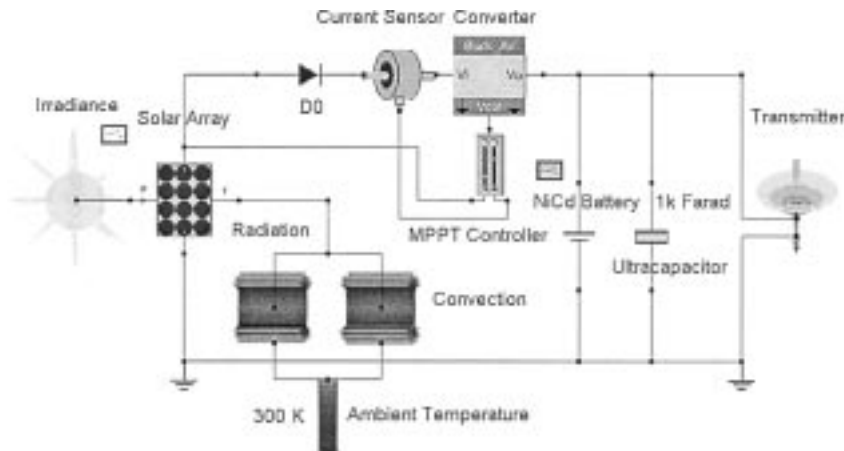


Fig. 8. Integrated photovoltaic power system in VTB computational environment for dynamic simulation and virtual prototyping.

TABLE III
INTEGRATED PHOTOVOLTAIC POWER SYSTEM SETUP

Model Name	Function	Specification
Solar Array	Primary energy source	80x10 (series by parallel) cells. Single silicon p^+n junction, with $R_s=11.3 \text{ m}\Omega$, $\gamma=1.0$, $\bar{\alpha}=0.305 \text{ A/W}$.
Ni/Cd Battery Array	Energy storage	20x15 cells, each 1.24 V, 24 Ah.
Ultracapacitor	Battery life and power extension	10x1000 cells, each 2.5 V, 10F
Transmitter	Pulsed power load	High 1 kW, low 0.25 kW, $D=0.5$, $f=0.05 \text{ Hz}$, load on/off =200s/250s
Converter	Averaged buck converter	
MPPT Controller	Maximum power point tracking controller	Incremental conductance algorithm
Irradiance	Solar irradiance model	Location: 34° N, 80° W. Time: June 21. Cloudless.
Radiation	Radiation cooling model	$\epsilon=1.0$, $A=8 \text{ m}^2$
Convection	Convection cooling model	$h_c=10 \text{ W/m}^2\text{K}$, $A=16 \text{ m}^2$
Ambient Temperature	Thermal Source	Ambient temperature

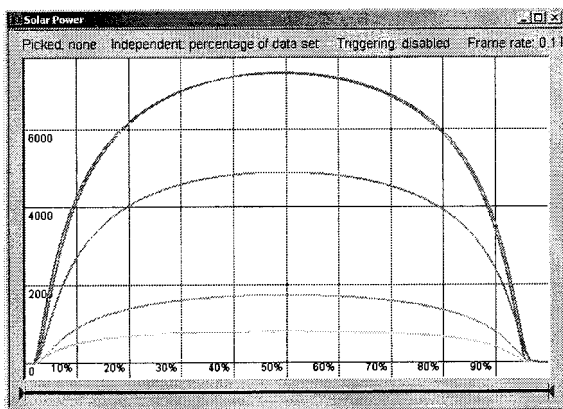


Fig. 9. Power (in watts) from solar array (from bottom to top): the electric output power, the radiated heat power, the convection heat power, the sum of electric and heat power, and the irradiated solar power.

the irradiated power. This is because the array releases some of its internal energy stored previously (temperature decrease). At any instant, the difference of the irradiated power and the sum of the output heat and electric power of the array is equal to the rate of the internal energy change.

For the same operating condition, Fig. 10 shows five curves for (from top to bottom) the temperature, the conversion efficiency, the current and the voltage of the solar array, and the state of charge of the battery respectively as a function of the time in seconds. The temperature of the solar array increases from 300 K (the ambient temperature) in the morning, and reaches its maximum 330.6 K at noontime. Then it decreases in the afternoon, and drops to the ambient temperature 20 min after sunset. Because the array is controlled by a maximum power point tracker, hence maximum conversion efficiency is achieved throughout the day, ranging between 10.9 to 12.2%. The efficiency curve also clearly shows the temperature effect: the highest efficiencies are obtained after sunrise and before sunset since the cell temperatures are low. At noontime, the high cell temperature results in lower maximum conversion efficiency. These characteristics can also be seen from the voltage and current curves, where higher array voltage corresponds to lower current (lower irradiance level and lower temperature) in order to extract maximum power.

The state of charge of the battery shows its interaction with the solar array and the load. The battery supplies full power to the load at night. It also shares part of the load demand in the early morning from sunrise to 6:45 AM and the late afternoon

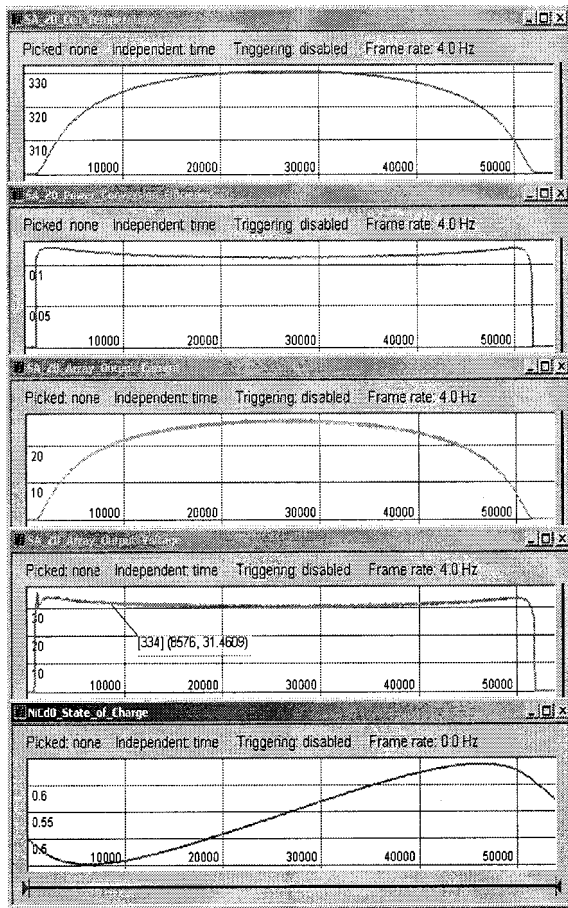


Fig. 10. Temperature (in degrees Kelvin), the conversion efficiency, the current (in amperes), and the voltage (in volts) of the solar array, and the state of charge of the battery as a function of time (in seconds).

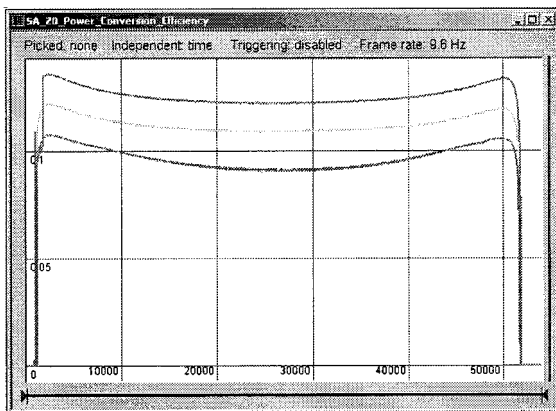


Fig. 11. Solar array energy conversion efficiencies as a function of time (in seconds) for three ambient temperatures: (from top to bottom) 280 K, 300 K, and 320 K.

from 6:00 PM to sunset, since the insolation level is low and the output power from the solar array is inadequate. Therefore the state of charge decreases. During the mid-day from 6:45 AM to 6:00 PM, plenty of power is available from the solar array, and the battery charges.

Figs. 11 and 12 show the solar array conversion efficiencies and the cell temperatures as a function of the ambient temperatures. Maintaining all other system setup the same, the highest

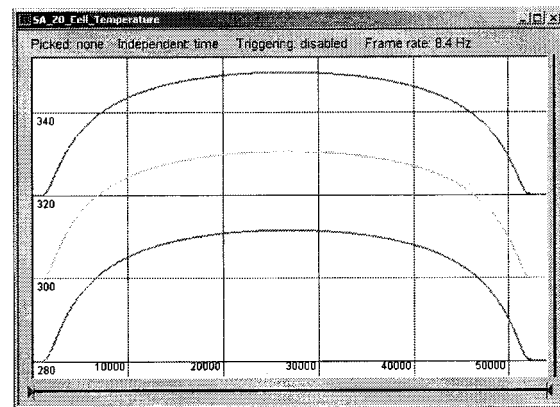


Fig. 12. Cell temperature variations (in degrees Kelvin) as a function of time (in seconds) in a day for three different ambient temperatures: (from bottom to top) 280 K, 300 K, and 320 K.

array maximum conversion efficiencies are 13.6%, 12.2% and 10.7% in the morning respectively for ambient temperatures of 280 K, 300 K, and 320 K, and the lowest maximum conversion efficiencies are 12.2%, 10.9%, and 9.0% correspondingly at noontime. The maximum cell temperatures at noontime are 311.5 K, 330.6 K, and 349.7 K (increased by 31.5 K, 30.6 K and 29.7 K) respectively for the ambient temperatures of 280 K, 300 K, and 320 K.

V. CONCLUSIONS

A solar array model based on the coupled multiphysics processes of photovoltaic energy conversion is built and implemented in virtual test bed computational environment. The terminals for natural power transport and conservation are defined so that interactions of the array system with the external world can be properly characterized by terminal variables. The approach to define terminal variables allows development of unified RC equations for all of the involved physical processes, therefore simultaneous solution for the system electrical potentials, temperatures and other terminal across variables is obtained. The static and dynamic behaviors of the solar array are simulated and the results show close match with the predictions of other work. The method to define the thermal terminal for natural heat transfer can be generalized to other physical processes where natural power transport and conservation are required.

REFERENCES

- [1] A. R. Hefner, "A dynamic electro-thermal model for the IGBT," in *Proc. IEEE IAS Ann. Meeting*, 1992, pp. 1094–1104.
- [2] A. R. Hefner and D. L. Blackburn, "Simulating the dynamic electro-thermal behavior of power electronic circuit and systems," in *Proc. IEEE Workshop Comput. Power Electron.*, 1992, p. 143.
- [3] G. Digele, S. Lindenkreuz, and E. Kasper, "Fully coupled dynamic electro-thermal simulation," *IEEE Trans. VLSI Syst.*, vol. 5, pp. 250–257, Sept. 1997.
- [4] P. E. Bagnoli, C. Casarosa, M. Ciampi, and E. Dallago, "Thermal resistance analysis by induced transient (TRAIT) method for power electronic devices thermal characterization—Part I: Fundamentals and theory," *IEEE Trans. Power Electron.*, vol. 13, pp. 1208–1219, Nov. 1998.
- [5] A. Ammous, K. Ammous, H. Morel, B. Allard, D. Bergogne, F. Selami, and J. P. Chante, "Electrothermal modeling of IGBT's: Application to short-circuit conditions," *IEEE Trans. Power Electron.*, vol. 15, pp. 778–789, July 2000.

- [6] G. Storti-Gajani, A. Brambilla, and A. Premoli, "Electrothermal dynamics of circuit: Analysis and simulations," *IEEE Trans. Circuits Syst.*, vol. 48, pp. 997–1005, Aug. 2001.
- [7] M. R. Lightner and S. W. Director, "Computer-aided design of electronic circuits," in *Electronics Engineers' Handbook*, 3rd ed, D. G. Fink and D. Christiansen, Eds. New York: McGraw-Hill, 1989, sec. 27.
- [8] R. A. Dougal, C. W. Brice, R. O. Pettus, G. Cokkinides, and A. P. S. Meliopoulos, "Virtual prototyping of PCIM systems—The virtual test bed," in *Proc. PCIM/HFPC '98 Conf.*, Santa Clara, CA, Nov. 1998, pp. 226–234.
- [9] M. B. Prince, "Silicon solar energy converters," *J. Appl. Phys.*, vol. 26, pp. 534–540, May 1955.
- [10] P. Rappaport, J. J. Loferski, and E. G. Linder, "The electron-voltaic effect in germanium and silicon p–n junctions," *RCA Rev.*, vol. 17, pp. 100–128, 1956.
- [11] J. J. Loferski, "Theoretical considerations governing the choice of the optimum semiconductor for photovoltaic solar energy conversion," *J. Appl. Phys.*, vol. 27, pp. 777–784, 1956.
- [12] P. Rappaport, "The photovoltaic effect and its utilization," *RCA Rev.*, vol. 20, pp. 373–397, Sept. 1959.
- [13] M. Wolf, "Limitations and possibilities for improvement of photovoltaic solar energy converters, Part I: Considerations for Earth's surface operation," *Proc. IRE*, vol. 48, pp. 1246–1263, July 1960.
- [14] F. A. Shirland, "The history, design, fabrication and performance of C_dS thin film solar cells," *Adv. Energy Conv.*, vol. 6, pp. 201–211, Oct.–Dec. 1966.
- [15] R. C. Neville, *Solar Energy Conversion: The Solar Cell*. New York: Elsevier, 1978.
- [16] B. E. A. Saleh and M. C. Teich, *Fundamentals of Photonics*. New York: Wiley, 1991, ch. 17.
- [17] M. P. Thekaekara, "Data on incident solar radiation," in *The Energy Crisis and Energy from the Sun*. New York: Institute of Environmental Sciences, 1974.
- [18] W. Shockley and W. T. Read, "Statistics of the recombinations of holes and electrons," *Phys. Rev.*, vol. 87, pp. 835–842, 1952.
- [19] R. Hall, "Electron–hole recombination in Germanium," *Phys. Rev.*, vol. 87, p. 387, 1952.
- [20] J. J. Wysocki and P. Rappaport, "Effect of temperature on photovoltaic solar energy conversion," *J. Appl. Phys.*, vol. 31, pp. 571–578, Mar. 1960.
- [21] B. K. Bose, P. M. Szczesny, and R. L. Steigerwald, "Microcomputer control of a residential photovoltaic power conditioning system," *IEEE Trans. Ind. Applicat.*, vol. IA21, pp. 1182–1191, Sept./Oct. 1985.
- [22] K. Zweibel and P. Hersch, *Basic Photovoltaic Principles and Methods*. New York: Van Nostrand Reinhold, 1984, ch. 5.
- [23] *VHDL Analog and Mixed-Signal Extensions*, IEEE Standards 1076.1-1999, Mar. 1999.
- [24] R. A. Dougal, S. Liu, and R. White, "Power and life extension of battery/ultracapacitor hybrids," *IEEE Trans. Comp. Packag. Technol.*, vol. 25, pp. 120–131, Mar. 2002.



Shengyi Liu (M'90) received the B.Sc. and M.Sc. degrees from Tsinghua University, Beijing, China, in 1985 and 1982, respectively, and the Ph.D. degree in electrical engineering from University of South Carolina, Columbia, in 1995.

Prior to joining the Department of Electrical Engineering, University of South Carolina, as a Research Professor he was Senior Research and Development Engineer from 1995 to 1999 at InnerLogic, Inc. His research interests include application and control study of solar energy conversion, fuel cells and electro-chemical capacitors for advanced power systems, modeling and simulation of interdisciplinary systems under virtual test bed computational environment. His interests also include modeling, design and applications of physical electronics-based devices, power semiconductor devices, and converters.



Roger A. Dougal (SM'90) received the B.S.E.E., M.S.E.E., and the Ph.D. degrees in electrical engineering from Texas Tech University, Lubbock, in 1978, 1980, and 1983, respectively.

He is Director of the Virtual Test Bed (VTB) Project (a multidisciplinary, multiuniversity effort to develop a comprehensive simulation and virtual prototyping environment for advanced power systems, integrating power electronics, electromechanics, electrochemistry, and controls into a common testbed). The VTB is unique in allowing the simulation of multidisciplinary systems by importing models from discipline specific source languages to a common workspace. In addition to modeling and simulation, his expertise includes power electronics, physical electronics, and plasmas.